Cusano, P., Palo, M., West, M. (2015): Long-period seismicity at Shishaldin volcano (Alaska) in 2003–2004: Indications of an upward migration of the source before a minor eruption. - *Journal of Volcanology and Geothermal Research*, *291*, p. 14-24.

DOI: http://doi.org/10.1016/j.jvolgeores.2014.12.008

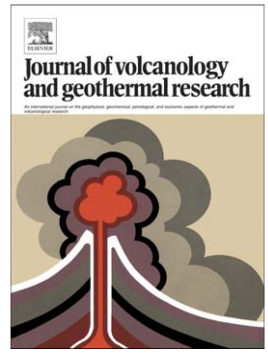

Long-period seismicity at Shishaldin volcano (Alaska) in 2003-2004: Indications of an upward migration of the source before a minor eruption

P. Cusano, M. Palo, M. West

PII: S0377-0273(14)00382-5
DOI: doi: 10.1016/j.jvolgeores.2014.12.008
Reference: VOLGEO 5462

To appear in: *Journal of Volcanology and Geothermal Research*

Received date: 3 June 2014
Accepted date: 9 December 2014

Long-period seismicity at Shishaldin volcano (Alaska) in 2003-2004: indications of an upward migration of the source before a minor eruption

Cusano P.[a,*], Palo M.[b], West M.[c]

[a]Istituto Nazionale di Geofisica e Vulcanologia - Sezione di Napoli, Osservatorio Vesuviano, Naples, Italy
[b]GeoForschungZentrum, Section 2.4, Potsdam, Germany
[c]Alaska Earthquake Center, Geophysical Institute, University od Alaska Fairbanks

Abstract

We have analyzed the long-period (LP) seismic activity at Shishaldin volcano (Aleutians Islands, Alaska) in the period October 2003 - July 2004, during which a minor eruption took place in May 2004, with ash and steam emission, thermal anomalies, volcanic tremor and small explosions. We have focused the attention on the time-evolution of LP rate, size, spectra and polarization dip angle along the dataset.

We find an evolution toward more shallow dip angles in the polarization of the waveforms during the sequence. The dip angle is a manifestation of the source location. Because the LP seismic sources are presumed to reflect the aggregation of gas slug or pockets within the melt, we use the polarization dip at the LP onset as a proxy for the nucleation depth of the seismic events within the conduit. We refer to this parameter as the nucleation dip and the position along the conduit of the gas aggregation as nucleation depth.

*Corresponding author. Tel: +390816108355; fax: +390816108351
Email address: paola.cusano@ingv.it (Cusano P.)

The nucleation dip changes throughout the dataset. It shows a sharp decrease between the end of December 2003 and the end of January 2004, followed by a gradual increase until the onset of the eruption. At the same time, a general increase of the LP rate occurs. We have associated the dip evolution with a sinking and a subsequent decrease of the nucleation depth, which would quickly migrate up to about 8 Km below the crater rim, followed by a slow depth decrease which culminates in the eruption.

The change in the nucleation depth reflects either a pressure variation within the plumbing system, which would affect the confining pressure experienced by the gas aggregations. We have imputed such a pressure change to the intrusion of batches of magma from a deeper magma chamber (< 10 km) toward a shallower one (> 5 km). For a cylindric conduit with rigid walls, this leads to a volume of the injected new magma of 10^5 - 10^7 m^3, compatible with estimates in other areas, suggesting that the LP process can be considered a good proxy of the thermodynamical conditions of the shallow plumbing system.

Keywords: Shishaldin volcano, long-period events, volcano seismicity, polarization, eruption precursors

1. Introduction

Among the several parameters observed in volcano monitoring, local seismicity is one of the most powerful and exploited. Earthquakes and tremors - induced by displacement of magma and associated gases - precedes and accompanies nearly all eruptions. These phenomena are very sensitive to the internal conditions of the volcano and the time-evolution of their properties

- such as energy and rate - reflect the evolution of the system when critical conditions are being approached.

Several authors have examined the relationship between seismicity and volcanic activity, with an emphasis on the rapid seismicity increases prior the eruption (Malone et al., 1983; Power et al., 1994; Aki and Ferrazzini, 2000; Alparone et al., 2003; Chastin and Main, 2003; Soosalu et al., 2005; Ruppert et al., 2011; De Martino et al., 2011b; Chouet and Matoza, 2012; Power et al., 2012; Sparks et al., 2012). Such a behavior has been associated with an overall increase of the stress within the plumbing system leading to an escalating fracturing process, which has been formally described by a second order differential equation ruling the time evolution of the density of earthquakes (Kilburn and Voight, 1998; Voight, 1988; Kilburn, 2003; Bell et al., 2011b). However, this framework is mainly valid for silicic volcanoes, where the seismicity is mostly induced by fracturing of the volcanic edifice, with the relevant presence of volcano-tectonic events. On the other hand, in volcanoes with low-density magmas, such as basaltic cases, the seismicity is mostly induced by the displacement of coherent gas aggregation nucleated in two-phase magmatic fluids. These conditions often create quasi-steady state seismicity pattern. In such cases, the seismicity is highly sensitive to changes in the conditions of the magmatic system (Bell et al., 2011a; De Martino et al., 2011b,a, 2012; Zecevic et al., 2013).

One of the most common seismic signature of the active volcanic areas is the presence of long-period (LP) events, characterized by a narrow frequency band (0.1-4 Hz) and produced by the interaction of flowing magmatic fluids and the conduit system. They have been detected all over the world and their source is now largely modeled as an inhomogeneity of the magma-gas mixture in the plumbing system leading to the aggregation of the gaseous phase. Such an aggregation may have the form of gas slugs or pocket, and ultimately produces a local pressurization of the system and an acceleration of the magmatic fluids (see, e.g., Chouet and Matoza, 2012, and references therein).

Due to the crucial role of the gaseous fraction, LP events are strongly affected by changes of the thermodynamic conditions within the plumbing system. Indeed the depth, the size and the recurrence of the gas aggregation are particularly sensitive to the local thermodynamic state of the system; system modifications will be reflected by changes of the waveform, wavefield properties and recurrence frequency of the LP events.

In this paper we analyze LP events occurring in the period 2003-2004 at Shishaldin volcano (Alaska, Figure 1). We examine the time-evolution of the occurrence rate, of the spectra, of the amplitude and of the polarization vector of the LP events in the period October 2003 - July 2004, which hosted a reactivation of the volcano including a small ash eruption. Our aim is to shine light on the internal processes before and during the eruption to understand how this volcanic system escapes from equilibrium conditions under certain external or internal inputs, which in turn is crucial for mitigating the volcanic risk. With this aim, we will infer insights into the thermodynamic changes occurring when the eruption is approaching, using the LP events as “detectors” of modifications of the state of the shallow plumbing system, in which these pressurization events are normally generated.

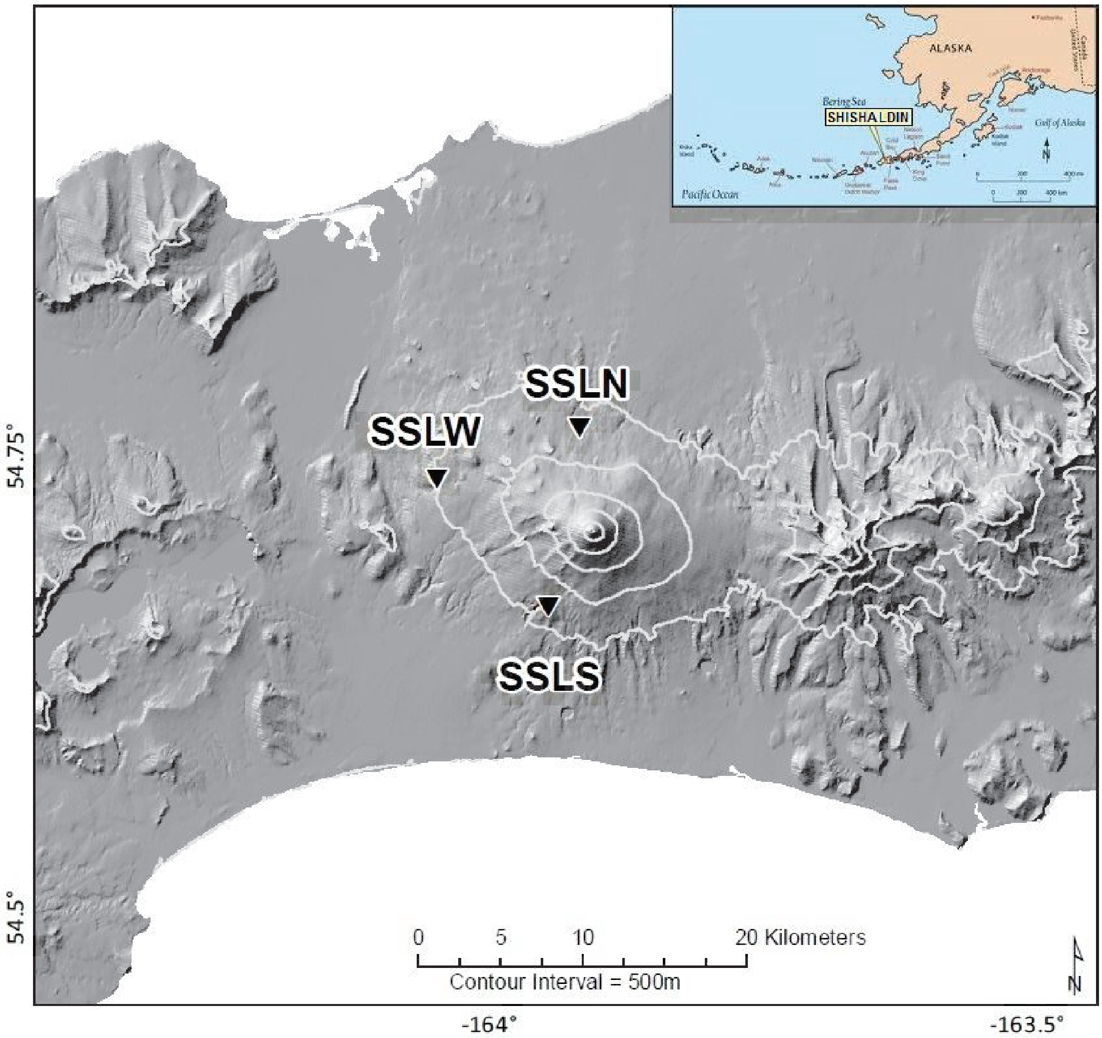

Figure 1: Map of Shishaldin volcano on Unimak Island, Alaska. Black triangles mark the locations of the seismic stations used in this study.

2. Shishaldin volcano

Shishaldin is a 2857 m-high stratovolcano on Unimak island, which is the Easternmost of the Aleutians Islands. It is the second most frequently active volcano of the archipelago, with nearly 40 eruptions in the last 250 years. A significant eruption sequence began in 1999, which consisted of a VEI (Volcanic Explosive Index) 3 sub-Plinian basaltic eruption followed by vigorous Strombolian activity (https:www.avo.alaska.edu/volcanoes/volcact.php?volcname=Shishaldin). Strong LP activity began about two months prior to the eruption. This activity was also present during the eruption and continued after for years. These LP events display a dominant frequency between 0.8 Hz and 2 Hz and a strong repetitiveness of the source mechanism, which creates classes of events sharing very similar waveforms (Caplan-Auerbach and Petersen, 2005; Petersen et al., 2006; Petersen, 2007). A time clustering has been detected as well, with most of the reported earthquakes clustered in few swarms, although so far only a small sub-set of all the occurring LP signals has been processes, as only high-energy events have been selected for the studies (Petersen, 2007).

Since 1999, the presence of a steam or gas plume has been nearly constant, and is likely associated in some fashion with ongoing LP process (Petersen et al., 2006). No comparable eruptions occurred in the several years following 1999. However, in the first months of 2004, the volcano reactivated, reaching the strongest phase of a minor eruption in May (VEI = 1). In January 2004 two thermal anomalies were observed near the summit in Moderate Resolution Imaging Spectroradiometer (MODIS) imagery (http://modis.gsfc.nasa.gov/) and in February several eyewitnesses noticed ash and steam emissions. Between the late April and the early May 2004, the seismicity intensified and volcanic tremor similar to that observed in the 1999 eruption appeared for the first time since then (Dixon et al., 2005; Neal et al., 2005, http://www.avo.alaska.edu/activity/avoreport_archives.php). In the same period, acoustic pressure sensors detected airwaves suggesting a shallowing of the tremor source (Petersen et al., 2006). On May 3 a thermal anomaly was revealed. Volcanic tremor continued, small explosions were recorded by the pressure sensors, and a weak intermittent thermal anomaly was observed in satellite images into the following summer. Low-level volcanic tremor continued through the end of the year. The last two ash and steam emissions were observed on September 24.

3. Data-set: picking of the LP events

The data-set used here consists of continuous recordings from October 17, 2003 to July 11, 2004, of ground velocity at three seismic stations (Figure 1). SSLS station, deployed on the southern flank of the volcano at a distance of 5.3 km from the summit, is equipped with a 2 Hz three-component Mark Products L-22 sensor. However, the EW component of this station malfunctioned in the study period and its signal is not fully reliable. The station on the north, SSLN, and that on the west side, SSLW, are vertical 1 Hz L-4C. They are placed at a station-summit distance of 6.3 km and 9.8 km, respectively. From each site, analog data is telemetered to Alaska Volcano Observatory (AVO) where it is digitized at 100 samples-per-second. We applied an instrument response correction and an acausal filter in the band 0.5-5 Hz to all data. In Figure 2 we show an example of an LP event recorded

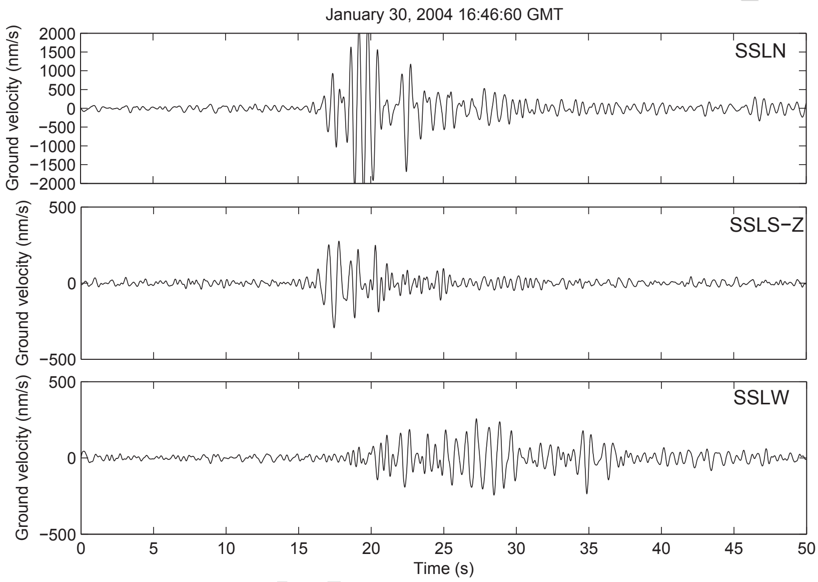

Figure 2: A Long Period earthquake recorded by the three Shishaldin seismic stations, SSLN on top, SSLS-Z (vertical component of SSLS) in the middle and SSLW on the bottom. The signals are filtered in the range 0.5-5 Hz.

by the three stations.

We used station SSLN to develop a catalog of LP events, since it has the best signal-to-noise ratio. Following De Martino et al. (2011b), we compute the maxima of the absolute value of the signal in two adjacent time-windows (sliding along the continuous recordings without overlapping) and detect an event when: 1. the ratio between the maximum of the first window and that of the second window exceeds a threshold, and 2. the amplitude of the second maximum is larger than four times the standard deviation of the background seismic signal averaged upon 1 h. The time-window and the threshold have been set empirically at 9 s and 1.7 s, respectively. Using this approach, about 330,000 events have been detected. For each, a 30-s time-window (centered

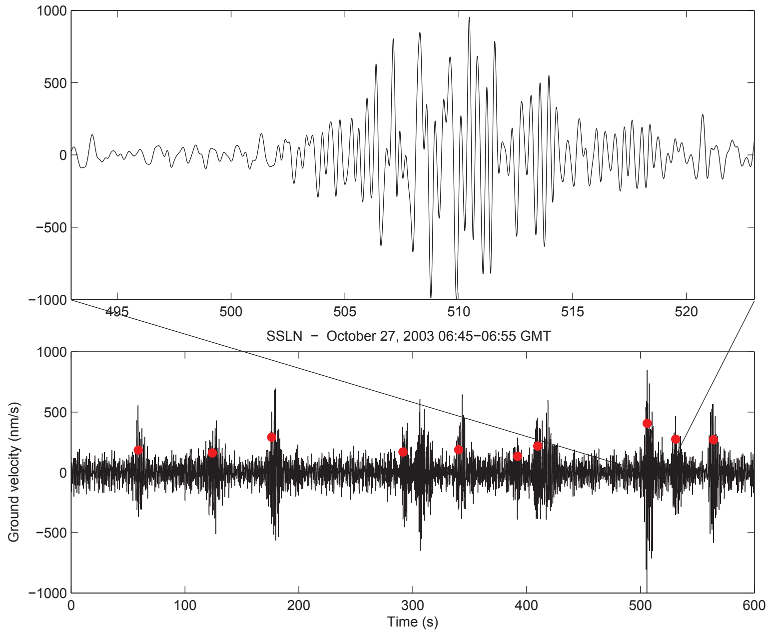

Figure 3: An example of the performance of the picking algorithm over a time windows of 600 seconds. On the bottom, each picked LP event is marked with a red asterisk. On the top, a zoomed view of one LP.

at the maximum detected amplitude of the waveform) has been extracted (Figure 3).

In Figure 4a we plot the time-evolution of the LP rate, calculated as the mean rate of events (per hour) in a day. From the beginning of the dataset to the end of December 2003, the LP rate shows a constant pattern (about 60 events/hour). It then increases until January 25, 2004 (about 75 events/hour). In the following phase, between about January 26 and April 25, the rate increases to about 85 events/hour and then returns to about 75 events/hour. This pattern is interrupted by the presence of a local minimum (less than 40 events/hour) between 11 and 19 of March. After April 26, 2004, the number of picked LP events diminishes drastically, and it remains on a very low level until the end of May (a minimum around 10 events/hour). In this time-interval, an increase of the background signal amplitude occurs (see Figure 5). As reported above, around the end of April, the volcanic tremor reappeared with characteristics similar to those observed during the eruption of 1999. The strong reduction of detected LP events can be due to a real reduction of the LP rate and/or to an increase of the background signal amplitude, which could cause small LP events to be hidden. After the end of May, the event rate stabilized around 45 events/hour, lower than the rate observed at the beginning of the dataset.

Based on these parameters and observed volcanic activity, we divide the dataset into five phases. Phase I: October 17-December 29, 2003; Phase II: December 30, 2003-January 24, 2004; Phase III: January 25 - April 25, 2004; Phase IV: April 26 - May 31, 2004; Phase V: June 1 - July 11, 2004. Phase IV includes the strongest phase of the eruption.

4. Seismic amplitude of LP events

As estimator of the LP size we evaluate the time-integral of the envelope of the extracted signals. In this way, we take into account the seismic radiation released along the entire duration of the event. The integral values are then averaged over blocks of six hours. In the following, we will refer to this observable with the term seismic amplitude. The time-evolution of the seismic amplitude at SSLN (black line) and at SSLS-NS (NS component of SSLS, red line) is plotted in Figure 4b. Similar patterns are observed at SSLS-Z (Z component of SSLS) and SSLW (not shown).

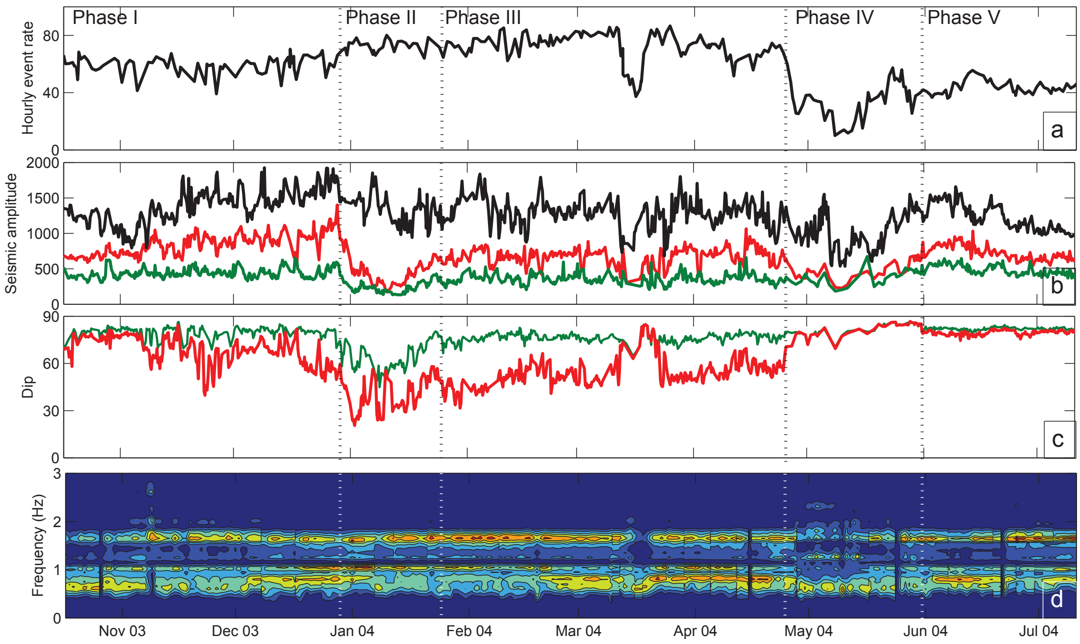

Figure 4: a) LP rate (events/hour); b) Seismic amplitude ([nm]) of the LP events recorded at SSLN (black line) and at SSLS-NS (red line), and of the seismic noise at SSLS-NS (green line); c) Nucleation (red line) and background signal (green line) dip; d) Spectrogram of LP events at SSLN. The vertical dotted lines separate the five phases described in the text. High-energy regional tectonic earthquakes have been manually excluded from the analyses.

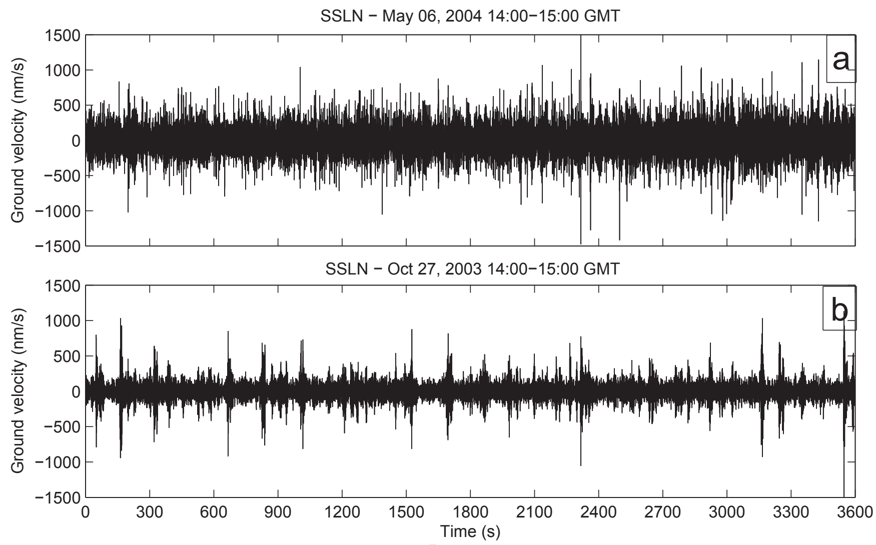

Figure 5: Two samples for SSLN showing the increase of volcanic tremor in Phase IV. Both the samples are frequency filtered in the 0.5-5 Hz band.

The seismic amplitude increases from the beginning of the dataset until the end of Phase I, when it reaches the largest value. It displays a minimum in Phase II and then follows a nearly linear pattern until the end of April 2004 (Phase III), except for the period March 11-19 when a minimum occurs. Afterwards, the seismic amplitude displays a sharp decrease lasting through Phase IV, while in Phase V it returns to the values observed at the beginning of the dataset.

We also estimate the seismic amplitude of the background signal using the first eight seconds of each extracted waveform. The seismic amplitude of the background signal (Figure 4b, green line) follows the same pattern of the LP events, except in Phase IV, when it shows an increasing amplitude that reaches its maximum value around the middle of May, 2004. This behavior agrees with indications of a strong volcanic tremor in this time interval.

5. Polarization analysis

To retrieve the properties of the polarization vector of the LPs, we use the algorithm of Kanasewich (1981). If a three-component station is available, this method allows to estimate the polarization vector by diagonalizing the covariance matrix constructed with the three ground motion components. The technique assumes that the eigenvector corresponding to the highest eigenvalue is the best estimate of the polarization vector. In general, the algorithm returns three parameters: the rectilinearity (RL), the azimuth (θ) and the dip (ϕ). RL is a measure of the linearity of the polarization trajectory, while the azimuth is the clockwise angle between the north direction and the polarization vector. The dip (also known as incidence angle or inclination) is the angle between the z axis and the polarization vector, with $\phi = 90°$ indicating horizontal oscillations and $\phi = 0°$ vertical oscillations. As the EW component of the three-component station is unreliable, the sole computable polarization parameter is the dip angle.

We estimate the dip angle in a 2s-long time window, sliding along the 30 s time window of the extracted LP events with a superposition of 75%. The time evolution of the dip shows a peculiar pattern common to all the LP events (Figs 6, 8). Dip angle is stable before the LP onset and then it decreases, reaching a minimum at the onset of the LP. During the event it increases gradually, reaching values $> 70°$, which indicates shallow oscillations. This pattern suggests a deep LP nucleation followed by an upward migration of the source towards the free surface. In this framework, we define the minimum of the dip curve as representative of the source depth of the pressurization phenomena that induces the LP events. For this reason, we refer to the nucleation dip as the minimum value of the dip curve, at the LP onset. We infer a correlation between this minimum dip and the nucleation depth of the seismic source. The particle motion in Figure 7 shows the behavior of the dip angle of the ground motion during the LP event, with the evolution from larger dip at the beginning of the event towards shallow oscillations at the end of the event. This analysis shows also that a dominant oscillation direction mostly exists even before the LP onset (although contaminated by scattered waves), confirming the reliability of the dip angles from the polarization analysis.

Although the dip angle follows a common pattern for all the LP events, the actual dip value and its recovery are different in each Phase. We identify one dominant class of dip behavior for each phase. In Figure 6 we show an example of the Phase I dip pattern. Panel a shows four curves displaying the dip averaged over all the LP events occurring in the four six-hour blocks belonging to the day October 28, 2003. Panels b and c show one of the LP events contained in the blocks (NS and vertical component, respectively). These curves demonstrate a stable dip value around 80° before the onset of the LP. We average this value over the first eight seconds to determine a mean dip of the background signal. After reaching a minimum at the LP onset, the dip increases and peaks in about 5 s.

Phase II (Fig. 8) is characterized by lower dip angles (60°-70°) at the beginning of the time window and nucleation dips of about 40°. In Phase III (Fig. 8), the dip of the pre-event signal assumes again higher values (70°-

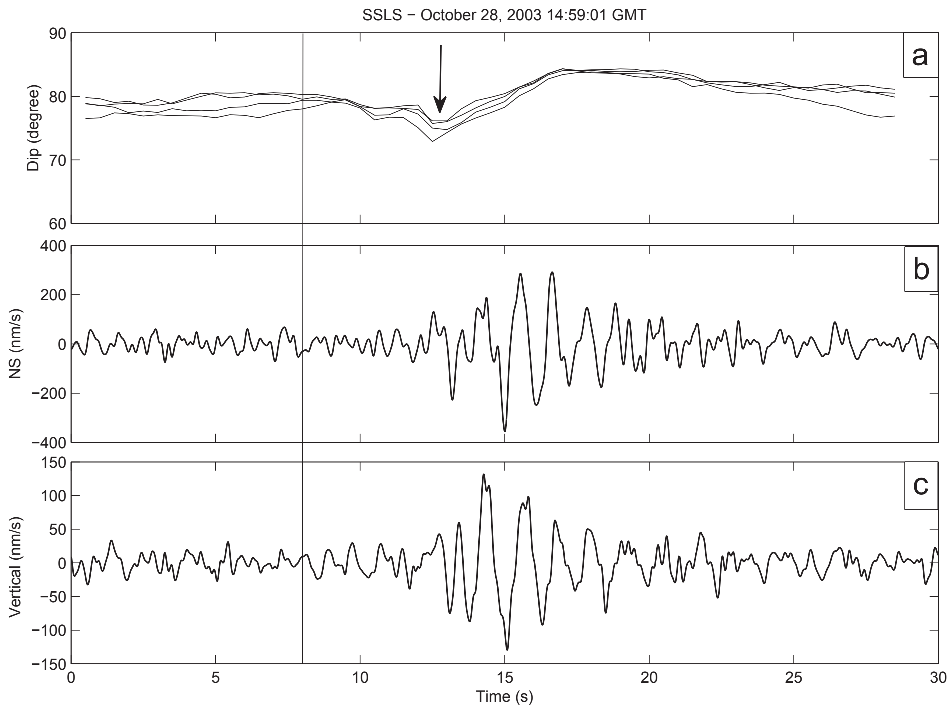

Figure 6: a) Dip angle curves estimated for October 28, 2003; b,c) one of the associated LP signal recorded by NS and Z component, respectively, of SSLS. The signals are frequency filtered in the band 0.5-5 Hz. The arrow highlights the nucleation dip assumed at the LP onset. The dip of the background signal is calculated as the mean value left of the vertical line.

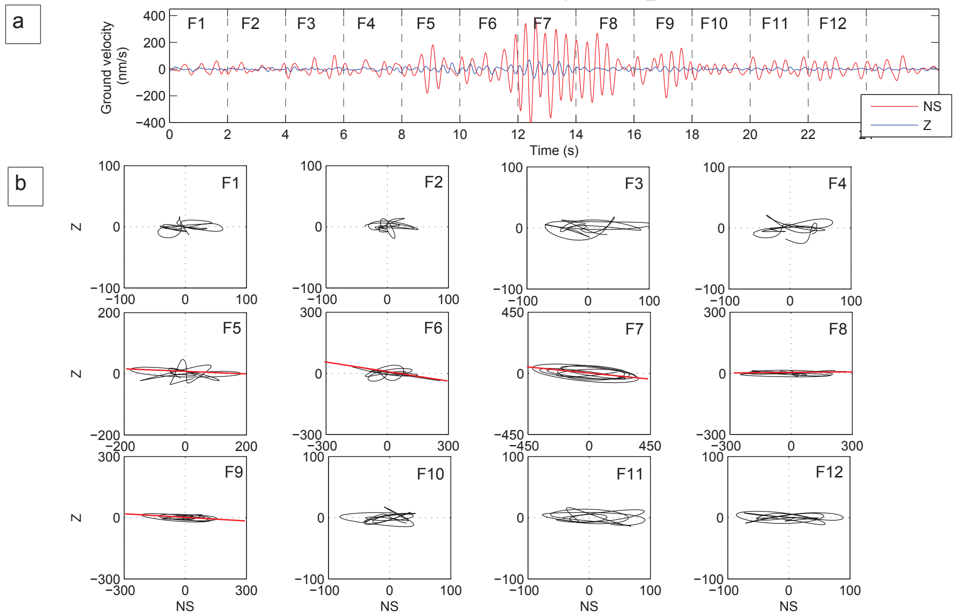

Figure 7: Example of NS-Z plane particle motion analysis performed over a signal of 24 s containing an LP event of Phase IV. Particle motion was calculated in 2s long time windows, without superposition. a) The NS and Z component of the signal used for the calculation, divided in 12 blocks of 2 s (F1-F12) by vertical dashed lines; b) The particle motion calculated over the 12 blocks.

80°), while the nucleation dip remains low (up to 50°). We have few data that were collect during the eruption (Phase IV, Fig. 8) on which to perform the analyses, but the results are quite stable. The dips remain high (about 80°-85°) along the signal without any evident minimum. This phenomenon is indicative of a very shallow and persistent source, and possibly of a dominant influence of volcanic tremor. The pattern in Phase V (Fig. 8) matches that of Phase I.

In Figure 4c, we plot the nucleation dip averaged over blocks of six hours (red line). The nucleation dip has a nearly constant value of about 80° during the first ~ 20 days of the data, which indicates a shallow source. Afterwards, the dip decreases slowly and irregularly into the beginning of Phase II. At the beginning of January the nucleation dip reaches a minimum around 30-40°, suggesting a deeper source, although wide oscillations superimpose on the overall trend. The dip increases during Phase III and Phase IV, reaching values around 85° at the end of the eruption, suggesting a steady upward migration of the nucleation depth as the eruption approaches. Moreover, the nucleation dip angle presents a maximum (about 85°) between 11 and 25 of March. During Phase V the dip values become again equal to about 80°, repeating the behavior exhibited during Phase I.

Figure 4c shows that the time history of dip parameter observed for the background signal mostly mimics that of the nucleation dip, but with higher values. In particular, during Phase IV the two curves basically overlap, suggesting that the sources of the two phenomena may be located at similar depths.

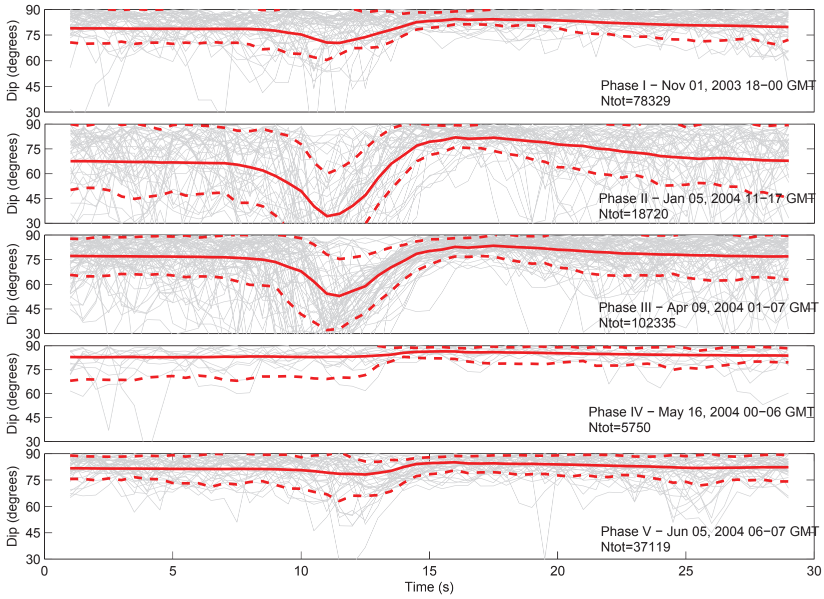

Figure 8: Each panel is relative to the Phase indicated in the bottom-right label. For each of them: Continuous red bold line represents the total mean dip curve estimated by averaging all the dip curves (Ntot) of the whole Phase; red dotted lines indicate the dispersion of the curves estimated as the standard deviation of the dip value at each time frame evaluating the events occurring within the 6-hour block indicated in the bottom-right label; light gray lines show the dip curves associated to the LPs of a one-hour-time interval belonging to the 6-hour block. We have estimated the dip dispersion over a block of 6 hours because the nucleation dip evolves on larger time scales and thus artificial larger dispersion can emerge. No sharp changes have been detected changing the selected 6-hour block. The variation of the nucleation dip on large time scales is also the reason why in same cases the mean dip curve does not fit exactly the stacked dip curves of the selected hour (we restricted the plot to the dip curves of one hour to make the figure more readable).

5.1. Uncertainties and assumptions

Throughout the paper we are assuming a straightforward connection between dip angle and source position. This assumption implies that the seismic wavefield is mostly composed of P waves. However, given the source-receiver distances (>5 km) and the stratified structure of the volcanic edifices a contribute from surface waves can be imaged. In that sense, the shallowing of the dip angle during an event could be at least favoured by the emergence of surface waves at the end of the LP event. In any case, the onset of the LP event should be dominated by source effects and we assume that in the nucleation phase the wavefield is mostly composed of P waves. On the other hand, other elements suggest that P waves could relevantly contribute also during the other stages of the events and thus that the dip increase is a real effect of an upward migration of a radiating source. In fact, the increase of the dip angle during an event is mostly gradual towards shallow oscillations, whereas a more scattered behaviour would be expected if a mix of surface and body waves would be present. Similarly, the particle motions show a rotation of the principal ground oscillation direction, while the superposition of waves with different polarizations should lead to a scattered motion hardly showing a preferential oscillation direction. Moreover, the mean dip found for the noise follows on average the time evolution of the nucleation dip, while the polarization dip should be basically constant if surface waves would dominate.

In volcanic areas, modifications of the source-induced dip angles can arise also from topographic effects, that is the interaction between the waves and the free surface. Following Neuberg and Pointer (2000), we infer this effect for three nucleation dips equal to 40°, 60° and 80°, which are roughly the values assumed at the end of Phase II, Phase III and Phase IV, respectively.

The inclination of the surface of volcano in correspondence of SSLS is about 20°, thus these three nucleation dips become respectively 20°, 40° and 60° respect to the normal to the volcano flank. Taking into account the pronounced conical symmetry of the edifice (Petersen et al., 2006) and the wavelengths typical of the LP seismicity (2.4 km and 1.9 km respectively for the frequencies 0.8 Hz and 1.6 Hz, assuming a medium velocity of 3 km/s (Dixon et al., 2005)), we can approximate the volcano profile as a triangular shape. In general the velocity model used for Shishaldin is a 1D model with horizontal layers (Dixon et al., 2005). In this case, considering a Vp/Vs ratio of 1.78 (Dixon et al., 2005) and a shallow source (about 500 m below the surface), dip angle distortions are relevant (3°-8°) only for angles of 80°-90° (60°-70° respect to the normal – Neuberg and Pointer (2000)).

The other factor of topographic distortion is eventually due to the surficial structure of the volcanic edifice combined with a shallow source. Since a detailed velocity model for Shishaldin does not exist, we can only take into account the simulation performed by Neuberg and Pointer (2000): the particle motion can suffer a distortion of 10°-20° for a surficial source (source depth of 1 km) and high frequencies (0.5-1 Hz).

Together with the topographic effect, which affects the individual dip estimate, one should also take into account the stochastic variability of the source process. This last factor induces a statistical variability of the dip behavior during each LP event. To account for this effect, we evaluate the standard deviation of the dip estimate, that is the error of the mean dip curves (continuous and dotted red curves in Fig. 8) for each Phase. Together with the variability of the source process, the dispersion of the dip values can include also the effect of random scattering of the medium, which can modify the measured dip angle even for a stable source.

In general, the standard deviation results relatively higher in correspondence of the nucleation dip, ranging between 5° in Phase V and 25° in Phase II. On the contrary, the standard deviation of the relative maximum of the dip curves is on average lower, with values in the range 5°-10°. These observations can be interpreted in terms of a larger variability of the source position during the LP nucleation, especially during Phase II, while the dip shallowing appears less variable. The error associated with the noise is 10°-20°.

Therefore, the statistical variations of the dip angles can be relevant (such as in Phase II) and thus must be considered dominant. These variations reflect into small-scale oscillations of the time evolution of the nucleation dip (Figure 4c). Nevertheless, the long-term increase and decrease of the nucleation dip indicate that the mean behaviour of the dip angle is anyway visible and meaningful and that the overall modifications of the source process overcomes the errors. In this sense, the nucleation dip can be considered a good proxy of the source depth. However, given the involved errors, we will mostly focus on the overall pattern of the nucleation dip and on its time variations, while the exact location of the source is behind the scope of the paper.

Finally, we should also mention that the calculated dip angles must be considered apparent dips (ϕ'), that is the projections of the real dips (ϕ) upon the Z-NS plane, as the EW component of the SSLS station is not available. Thus, to be able to connect the dip angles to the depth source, we are implicitly assuming that the source does not change its position over the NS-EW plane (or at least that the angle between the line connecting the source and the SSLS station and the North direction is constant). This assumption is well grounded as the activity of Shishaldin has been historically located in the crater area, which can be considered as a point source given the distance between the crater. Given the angle between the North direction and the line connecting the crater and SSLS ($\beta \sim 20°$), the discrepancy between real and apparent dip is $\lesssim 2°$ ($\frac{tan(\phi')}{tan(\phi)} = cos\beta$), thus negligible.

6. Spectral analysis

To evaluate the spectral content of the analyzed dataset we calculated the power spectrum of the extracted LP events. In detail, we estimate the square of the Fast-Fourier Transform (FFT) of each event windowed with a Hanning function. For this analysis, the signals were corrected for the instrumental response and filtered in the band 0.5-10 Hz.

Figure 4d illustrates the time evolution of the LP power spectra along the whole dataset at SSLN. The spectrograms of SSLS and SSLW are plotted in Fig. 9. Each bin displays the normalized spectra (the spectrum of each LP is normalized with respect to its own maximum) averaged over 6-hour blocks.

The spectra of all the stations appear composed of two main peaks, one at 0.8-1 Hz and another at 1.3-1.6 Hz, indicating a major imprinting of source effects on the waveforms. Nevertheless, these two broad peaks can be, in same cases, subdivided in two or more peaks; their relative amplitude depends on the station. In detail, SSLN shows two peaks around 0.8 Hz and

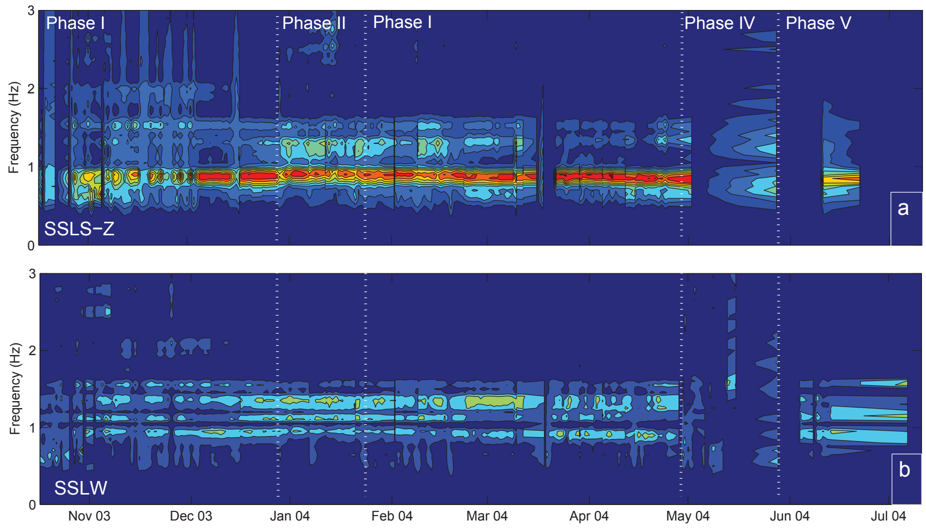

Figure 9: Normalized spectrogram of LP events at SSLS-Z (a) and at SSLW (b). The vertical dotted lines separate the five phases described in the text. To process the LP waveform at each station the picking procedure has been computed separately for each station, with the effect that low-energy events may evade detection at SSLS and SSLW.

1 Hz and a strong component around 1.6 Hz, whereas for SSLW and SSLS the component at 1.4 Hz and 0.9 Hz dominate, respectively.

The spectra appear rather stable along the phases, with just a possible redistribution of the energy among the peaks. During Phase IV, a remarkable increase of a component at 0.6-0.8 Hz is visible. Such a component is also observed in the brief time interval between March 11 and 25.

7. Discussion and conclusions

In this paper, we have analyzed the seismicity of Shishaldin volcano (Alaska) in the period 2003-2004, which includes a small ash and steam eruption culminating in May 2004. We focus on long-period (LP) events, which occurred with a rate of 20-80 events/hour and have a spectral content in the 0.5-3 Hz range.

We have extracted a very large dataset of LPs (about 330,000), picked by a revised version of the short-term average/long-term average (STA/LTA) method at the station with the highest signal-to-noise ratio. These LPs show variations in amplitude, spectra and particle motion that reveal the systematic evolutions in generating plumbing system.

The dip angles from polarization analysis increase during the LP events nearly linearly from a minimum value at the onset of the event towards shallow oscillations, suggesting an upward migration of the LP source, consistent with observation elsewhere (Chouet, 2003; Palo et al., 2009; Kumagai et al., 2011). We have associated this minimum value with the depth at which the LP events nucleate. We define as ΔP the local pressure dishomogeneity within the magma-gas mixture in the shallow feeding network leading to the LP events. Specifically, one can depict this framework as a pressure gradient between a coherent gas aggregation and the surrounding magma and/or hydrothermal system. ΔP induces an acceleration of the fluid, which interacts with the rock radiating seismic waves under the form of LP events.

We have also estimated the dip parameter for the background signal, which appears systematically higher than the nucleation dip. Moreover, its time evolution follows the nucleation dip. These behaviors suggest that some of the background signal may also have a volcanic origin, possibly suggesting permanent degassing. This scheme would be similar to many other volcanoes worldwide showing a background volcanic tremor on which intermittent high-energy volcanic quakes are superimposed (Julian, 1994; Chouet, 1996; Bottiglieri et al., 2005; De Lauro et al., 2008, 2009; Palo and Cusano, 2013). The shallowest dips of both the LPs and tremor (>80°) overlap during the eruption (Phase IV), suggesting that the two phenomena somehow merge into a unique continuous signal (also supported by the similar amplitudes in this Phase). This phenomenon often appears in volcanoes close to or during an eruption (e.g., Chouet et al., 1994; De Martino et al., 2011a).

The nucleation dip evolves from an initial value of 75° at the beginning of our dataset. It decreases to a minimum of about 30°-40° shortly before the middle of January 2004, in Phase II, though there is considerable scatter at this time. After this, the dip increases slowly until the eruption (May, 2004). At this point it increases from about 60° at the end of Phase III to about 85° during Phase IV. After the eruption (Phase V), the nucleation dip returns to values around 75°, similar to those found at the beginning of the dataset.

This gradual change of the nucleation dip suggests an analogous change of the nucleation depth. Assuming a nearly vertical main conduit composed of a homogeneous medium and conducting purely compressional waves, a rough estimate of the nucleation depth gives values of about 0.9 km, 3.0 km and 6.3 km respectively for dip of 80°, 60° and 40° respect to SSLS, which has an elevation of about 2 km below the crater. Although our depth estimates are highly approximated, they are, on average, deeper than those found by Petersen et al. (2006), who estimated LP depths at 0–3 km below the crater.

However, our estimates should be considered deeper limits, as a more realistic velocity model would probably imply layers with velocities increasing with the depth, which would reduce the depth at which the backtraced seismic ray crosses the vertical conduit. This is especially true for the depth estimate corresponding to the highest dip, as topography effects in this case can be strong and dip angles close to 90° might be basically induced by any source at depths between 0.9 km below SSLS and the free surface. Despite these limitations, we cannot exclude that these differences are the signature of the peculiar seismic activity just before the eruption, as opposed to the activity when the volcano is in steady state (Petersen et al., 2006).

Dividing our estimates of the nucleation depth by the rise time of the dip during an LP event ($\sim$ 5s), we obtain rising velocities of about 0.2-1 Km/s. Assuming that compressive waves radiated from the source dominate the wavefield during the whole LP event, these values are compatible with a pressure wave propagating along the conduit towards the surface, rather than to the upward migration of the gas aggregation (Ishihara, 1985; Palo et al., 2009).

Our findings imply that the LP source is at first relatively shallow ($\lesssim$1 km respect to SSLS), than it deepens until reaching about 3.0 km below SSLS at the end of Phase I and about 6.3 km during Phase II. Afterwards, it moves upwards again, reaching depths of about 3.0 km at the end of Phase III. At the beginning of Phase IV, the dip suggests a source nearly as shallow as that observed during Phase I. Later in Phase IV, there is a slight increase of the dip, suggesting a shallowing, until it becomes basically surficial. After the eruption, the source depth becomes again stabilized at around 1 km, as in Phase I.

This variable nucleation depth indicates that the source of LP events may shift within the conduit (or, more in general, along the plumbing system) in a nearly continuous way. This implies that structural effects, such as physical constraints that promote gas accumulation (inclined conduits, roofs, asperities, etc.), are negligible in the ΔP nucleation and thus in the LP production. Source mechanisms such as chocked fluid flow (e.g., Petersen, 2007) seem unlikely. A more probable mechanism for LP generation includes spontaneous gas aggregation in the form of slags or pockets (Bottiglieri et al., 2005). Acoustic measurements and visual observation of gas puffing from the crater indicate that Shishaldin can host such source mechanisms (Vergniolle et al., 2004; Caplan-Auerbach and Petersen, 2005). If this is true, then changes of the source position, as well as other LP properties, are likely manifestation of thermodynamical changes in the plumbing system. The LP source is surprisingly persistent despite its migrating location in agreement with the LP rate pattern. The LP production, that shows an inhibition while a high-energy volcanic tremor appears in Phase IV, restarts in Phase V, indicating that the eruption does not destroy the LP source process.

The persistence of the LP source process is also confirmed by the spectral analysis, which shows rather stable frequency content along the dataset. Two main spectral peaks in the frequency bands 0.8-1 Hz and 1.3-1.6 Hz at all the stations suggest that the LP waveforms are dominated by steady source mechanisms. The nearly common spectral bands among the stations suggest that these mechanisms should include an imprinting of the source process. On the other hand, the details of the spectra show a dependence on the station, with a variation of the frequency of the main peaks and of the distribution of the energy among the peaks. This evidence together with the stability over time of the spectra suggest also a relevant contribution of site and path effects, which are less sensitive to modifications of the source position and of the thermodynamical conditions of the fluid-rich volcanic conduit hosting the LP activity and feeding the external emissions.

The reduction of the seismic amplitude during Phase IV agree with a persistent gas-driven source. The low amplitude may reflect that the gas fraction is predominantly driving the eruption instead of discrete seismic events. This would also explain why at the end of the eruption there is a gradual recover of the LP rate and amplitude.

Moving from Phase I to Phase II, there is a decrease in the seismic amplitude and the dip. Considering the estimates of the source depth reported above, this transition corresponds to a deepening of the source from about 3.0 km to about 6.3 km below SSLS. The attenuation effects associated with this sinking of the source can be calculated, taking into account geometric spreading and scattering effects:

$$\frac{A_{II}}{A_I} = \frac{x_I}{x_{II}} e^{\frac{f\pi}{Qv}(x_I - x_{II})} \tag{1}$$

where $A_{I,II}$ and $x_{I,II}$ are, respectively, the signal amplitude and the station-source distance in the Phase I and Phase II. Fixing the frequency at 1 Hz and adopting typical parameters for volcanic areas of the quality factor and the wave velocity (Q=30-100, v_P=1–3 km/s Benoit and McNutt (1997); Kumagai and Chouet (1999); Morrissey and Chouet (2001); Dixon et al. (2005)), the attenuation falls in the range 15 % - 40 %. In our case, the amplitude drops by about 50 % - 70 %, depending on the station, suggesting that attenuation effects could combine with a real decrease of the energy of the source process.

Thus, we can claim that the most prominent changes of the parameters occur in Phase II, as confirmed also by a thermal anomaly recorded in January. We hypothesize that in Phase II 1) changes of nucleation depths indicate a change of the source position, reflecting in turn modifications of the thermodynamic state within the plumbing system and 2) a sinking of the source reflects a decrease of the confining pressure within the plumbing system, allowing the nucleation at greater depths. In this framework, similarly the source shallowing during Phase III would be the effect of an increase of the pressure, which would lead the ΔP to nucleate upper and upper to find suitable conditions to overcome to the confining pressure. Such an increase of pressure and an upward migration of the source of seismicity are plausible before the eruptions and observed at many volcanoes worldwide (e.g., Castellano et al., 1993; Voight et al., 1998; Sparks, 2003; Battaglia et al., 2005; Sparks et al., 2012; Jousset et al., 2013).

Under these hypotheses, it is possible to infer a rough estimate of the internal pressure change that drives the source as it migrates upwards from the end of Phase II (when the source depth h is maximum - $h_{II} \sim 6.3km$) to the end of Phase III ($h_{III} \sim 3.0km$), which begins the eruption. We define such a pressure change as $\Delta\overline{P}$. We adopt a simple hydrostatic model, in which the changes of the depths of the LP source are only due to changes of the mean pressure within the plumbing system, acting as confining pressure for the gas aggregations. We assume that the volcanic crises is induced only by a pressure variation, leaving unchanged all the other parameters (temperature, gas content, etc.). In this scheme, starting from the depth estimations introduced above, the change of hydrostatic pressure $\rho g(h_{III} - h_{II})$ would equal the change of internal pressure. Therefore, adopting a value of the mean magma density (assumed constant) typical of a melt-gas mixture (ρ=1500 kg/m^3, Ripepe and Gordeev (1999); Mori and Burton (2009)), we find a $\Delta\overline{P} \sim 5\times10^{7}$ Pa. This value can be connected with the variation of density via:

$$\frac{d\rho}{\rho} = \frac{\Delta\overline{P}}{K} \tag{2}$$

which, assuming rigid conduit walls, can be linked to the mass change, leading to the pressure variations:

$$\frac{\Delta M}{M} = \frac{\Delta\overline{P}}{K} \tag{3}$$

where K is the bulk modulus. For a cylindric conduit, M= $\pi\ R^2\ l\ \rho$, where l is the length of the conduit (l ~3 km) and R its radius (fixed to 6 m, Vergniolle et al. (2004)). For rhelogical parameters typical of bubbly magma (K=10^{6}-10^8 Pa, ρ=1500 kg/m^3, Ripepe and Gordeev (1999); Nishimura (2009)), we get a value of ΔM ~10^{8} - 10^{10} kg, occupying a volume of ΔV ~10^{5} - 10^{7} m^3. Although these values must be considered reliable only to an order of magnitude, they are compatible with other estimates of emitted material during larger eruptions, such as the 1999 Shishaldin (Stelling et al., 2002) and of 2007 Stromboli (Landi et al., 2009) eruption, estimated around $10^7 m^3$. This suggests that the location of LP events, even if roughly inferred from polarization dip, can be very useful to our goal of mitigating volcanic risk. In particular, rather than the absolute location of the events, relevant for volcanic risk purposes is the source depth variation, which can be roughly (and potentially in real-time) inferred also at volcanoes with poor instrumental monitoring, even with only one three-component seismometer, as we have shown.

Geodetic observations during the eruption of 1999 suggest that the main magma chamber at Shishaldin is not shallow ($\lesssim$10 km, Moran et al. (2006)). On the other hand, the presence of some magma at shallow depth ($\sim 3-5$ km, possibly coexisting with an hydrothermal system) is indicated by geochemical and seismological evidences (Stelling et al., 2002; Vergniolle and Caplan-Auerbach, 2004; Moran et al., 2006) and by the persistent gas plumes of sulfurous nature (Caplan-Auerbach and Petersen, 2005). Moran et al. (2006) suggest that magma migrated from the deeper chamber to the shallower chamber with a velocity of $\sim$80 m/day during the eruption of 1999.

Therefore, we hypothesize the existence of a shallow plumbing system, with mostly degassed magma, at low pressure (and possibly interacting with a hydrothermal system), and a deeper plumbing system at higher-pressure conditions, hosting low-degassed magma. The deeper chamber can still host magma with properties similar to those of the magma erupted during the event of 1999; this magma is basaltic and able to produce strombolian fountains at shallow depths, where its volatile components can be released (Nye et al., 2002; Stelling et al., 2002).

We propose that the activation of a path between the shallow and the deep magma chamber is responsible for the overall downward and the subsequent upward migration of the LP events. In this case, the lower plumbing system would experience a temporary pressure drop favoring the gas nucleation also at larger depths, thus explaining the general dip reduction in Phase I-II. It also explains the strong dip fluctuations, as pressurization events could nucleate at more than one depth before the two subsystems clear the pressure discontinuity becoming one. Afterwards, magma from the deeper sector migrates upwards slowly increasing the overall pressure and reducing the thermodynamic inhomogeneities in the plumbing system, which are eventually removed by the eruption.

The connection path could be promoted by the high-pressure low-degassed deep magma pushing against the upper structure. From this pushing, a part of the volatile fraction of the magma can exsolve and flush upwards, increasing the density of gas in the upper chamber visible as an increase of the LP amplitude during Phase I. On the contrary, the pressure increase in Phase III would be induced by the upward migrations of batches of deep magma, with the consequence of a larger and larger release of gas, which in turn makes higher the internal pressure and the LP rate. When the internal pressure reaches critical conditions, the eruption starts.

In our scheme the transient phenomenon occurred between March 11 and 25 remains unexplained. The behavior of the estimated parameters (lowering of event rate and seismic amplitude, and decreasing dip angles) indicates a decrease of the nucleation depth by mean of a mechanism similar to that explaining the eruptive Phase. Visual inspection of the waveforms indicates that decreased event rate and seismic amplitude are real changes and not an artifact of increasing tremor. This suggests a temporary reduction in degassing. The absence of observer reports during this time period makes it impossible to confirm this assertion.

Nevertheless, our work highlights the importance of observing the pressurization phenomena generated by active volcanoes as a tool for inspecting the internal conditions of the shallow plumbing system. In the case of Shishaldin, variations in the LP process began at least three months before the 2004 eruption. This study demonstrates the potential for interpreting modest changes in LP earthquakes properties to infer specific physical changes in magmatic system. If assessed quickly, this types of changes may prove useful for establishing the likelihood and timing of potential eruptions.

Bibliography

Aki, K., Ferrazzini, V., 2000. Seismic monitoring and modeling of an active volcano for prediction. Journal of Geophysical Research 105 (B7), 16617–16.

Alparone, S., Andronico, D., Lodato, L., Sgroi, T., 2003. Relationship between tremor and volcanic activity during the southeast crater eruption on mount etna in early 2000. Journal of geophysical research 108 (B5), 2241.

Battaglia, J., Ferrazzini, V., Staudacher, T., Aki, K., Cheminée, J.-L., 2005. Pre-eruptive migration of earthquakes at the piton de la fournaise volcano (réunion island). Geophysical Journal International 161 (2), 549–558.

Bell, A. F., Greenhough, J., Heap, M. J., Main, I. G., 2011a. Challenges for forecasting based on accelerating rates of earthquakes at volcanoes and laboratory analogues. Geophysical Journal International 185 (2), 718–723.

Bell, A. F., Naylor, M., Heap, M. J., Main, I. G., 2011b. Forecasting volcanic eruptions and other material failure phenomena: an evaluation of the failure forecast method. Geophysical Research Letters 38 (15), L15304.

Benoit, J. P., McNutt, S. R., 1997. New constraints on source processes of volcanic tremor at arenal volcano, costa rica, using broadband seismic data. Geophysical Research Letters 24 (4), 449–452.

Bottiglieri, M., De Martino, S., Falanga, M., Godano, C., Palo, M., 2005. Statistics of inter-time of strombolian explosion-quakes. EPL (Europhysics Letters) 72 (3), 493.

Caplan-Auerbach, J., Petersen, T., 2005. Repeating coupled earthquakes at shishaldin volcano, alaska. J. Volcanol. Geotherm. Res.

Castellano, M., Ferrucci, F., Godano, C., Imposa, S., Milano, G., 1993. Upwards migration of seismic focii: A forerunner of the 1989 eruption of mt etna (italy). Bulletin of volcanology 55 (5), 357–361.

Chastin, S. F., Main, I. G., 2003. Statistical analysis of daily seismic event rate as a precursor to volcanic eruptions. Geophysical research letters 30 (13).

Chouet, B., 2003. Volcano seismology. Pure and Applied Geophysics 160 (3-4), 739–788.

Chouet, B. A., 1996. Long-period volcano seismicity: its source and use in eruption forecasting. Nature 380 (6572), 309–316.

Chouet, B. A., Matoza, R. S., 2012. A multi-decadal view of seismic methods for detecting precursors of magma movement and eruption. Journal of Volcanology and Geothermal Research 252, 108–175.

Chouet, B. A., Page, R. A., Stephens, C. D., Lahr, J. C., Power, J. A., 1994. Precursory swarms of long-period events at redoubt volcano (1989–1990), alaska: Their origin and use as a forecasting tool. Journal of Volcanology and Geothermal Research 62 (1), 95–135.

De Lauro, E., De Martino, S., Del Pezzo, E., Falanga, M., Palo, M., Scarpa, R., 2008. Model for high-frequency strombolian tremor inferred by wave-field decomposition and reconstruction of asymptotic dynamics. Journal of Geophysical Research 113 (B2), B02302.

De Lauro, E., De Martino, S., Falanga, M., Palo, M., 2009. Modelling the macroscopic behavior of strombolian explosions at erebus volcano. Physics of the Earth and Planetary Interiors 176 (3), 174–186.

De Martino, S., Errico, A., Palo, M., Cimini, G., 2012. Explosion swarms at stromboli volcano: A proxy for nonequilibrium conditions in the shallow plumbing system. Geochemistry, Geophysics, Geosystems 13 (3).

De Martino, S., Falanga, M., Palo, M., Montalto, P., Patanè, D., 2011a. Statistical analysis of the volcano seismicity during the 2007 crisis of stromboli, italy. Journal of Geophysical Research 116 (B9), B09312.

De Martino, S., Palo, M., Cimini, G., 2011b. A statistical study of the stromboli volcano explosion quakes before and during 2002–2003 eruptive crisis. Journal of Geophysical Research: Solid Earth (1978–2012) 116 (B4).

Dixon, J. P., Stihler, S. D., Power, J. A., Tytgat, G., Estes, S., Prejean, S., Snchez, J. J., Sanches, R., McNutt, S. R., Paskievitch, J., 2005. Catalog of earthquake hypocenters at alaskan volcanoes: January 1 through december 31, 2004. Tech. rep., USGS.

Ishihara, K., 1985. Dynamical analysis of volcanic explosion. Journal of geodynamics 3 (3), 327–349.

Jousset, P., Budi-Santoso, A., Jolly, A. D., Boichu, M., Dwiyono, S., Sumarti, S., Hidayati, S., Thierry, P., et al., 2013. Signs of magma ascent in lp and vlp seismic events and link to degassing: An example from the 2010 explosive eruption at merapi volcano, indonesia. Journal of Volcanology and Geothermal Research 261, 171–192.

Julian, B. R., 1994. Volcanic tremor: nonlinear excitation by fluid flow. Journal of Geophysical Research: Solid Earth (1978–2012) 99 (B6), 11859–11877.

Kanasewich, E. R., 1981. Time Sequence Analysis in Geophysics. Univ. of Alberta Press.

Kilburn, C. R., 2003. Multiscale fracturing as a key to forecasting volcanic eruptions. Journal of Volcanology and Geothermal Research 125 (3), 271–289.

Kilburn, C. R., Voight, B., 1998. Slow rock fracture as eruption precursor at soufriere hills volcano, montserrat. Geophysical Research Letters 25 (19), 3665–3668.

Kumagai, H., Chouet, B. A., 1999. The complex frequencies of long-period seismic events as probes of fluid composition beneath volcanoes. Geophysical Journal International 138 (2), F7–F12.

Kumagai, H., Placios, P., Ruiz, M., Yepes, H., Kozono, T., 2011. Ascending seismic source during an explosive eruption at tungurahua volcano, ecuador. Geophysical Research Letters 38 (1).

Landi, P., Corsaro, R., Francalanci, L., Civetta, L., Miraglia, L., Pompilio, M., Tesoro, R., 2009. Magma dynamics during the 2007 stromboli eruption (aeolian islands, italy): mineralogical, geochemical and isotopic data. Journal of Volcanology and Geothermal Research 182 (3), 255–268.

Malone, S. D., Boyko, C., Weaver, C. S., 1983. Seismic precursors to the mount st. helens eruptions in 1981 and 1982. Science 221 (4618), 1376–1378.

Moran, S., Kwoun, O., Masterlark, T., Lu, Z., 2006. On the absence of insar-detected volcano deformation spanning the 1995–1996 and 1999 eruptions of shishaldin volcano, alaska. Journal of volcanology and geothermal research 150 (1), 119–131.

Mori, T., Burton, M., 2009. Quantification of the gas mass emitted during single explosions on stromboli with the so2 imaging camera. Journal of Volcanology and Geothermal Research 188 (4), 395–400.

Morrissey, M., Chouet, B., 2001. Trends in long-period seismicity related to magmatic fluid compositions. Journal of volcanology and geothermal research 108 (1), 265–281.

Neal, C. A., McGimsey, R. G., Dixon, J., Melnikov, D., 2005. 2004 volcanic activity in alaska and kamchatka: Summary of events and response of the alaska volcanoobservatory. Tech. rep., USGS.

Neuberg, J., Pointer, T., 2000. Effect of volcano topography on seismic broad-band waveforms. Geophysical Journal International 143, 239–248.

Nishimura, T., 2009. Ground deformation caused by magma ascent in an open conduit. Journal of Volcanology and Geothermal Research 187 (3), 178–192.

Nye, C., Keith, T., Eichelberger, J., Miller, T., McNutt, S., Moran, S., Schneider, D., Dehn, J., Schaefer, J., 2002. The 1999 eruption of shishaldin volcano, alaska: monitoring a distant eruption. Bulletin of volcanology 64 (8), 507–519.

Palo, M., Cusano, P., 2013. Wavefield decomposition and phase space dynamics of the seismic noise at volcàn de colima, mexico: evidence of a two-state source process. Nonlinear Processes in Geophysics 20, 71–84.

Palo, M., Ibáñez, J., Cisneros, M., Bretón, M., Del Pezzo, E., Ocaña, E., Orozco-Rojas, J., Posadas, A., 2009. Analysis of the seismic wavefield properties of volcanic explosions at volcán de colima, méxico: insights into the source mechanism. Geophysical Journal International 177 (3), 1383–1398.

Petersen, T., 2007. Swarms of repeating long-period earthquakes at shishaldin volcano, alaska, 2001–2004. Journal of Volcanology and Geothermal Research 166 (3), 177–192.

Petersen, T., Caplan-Auerbach, J., McNutt, S. R., 2006. Sustained long-period seismicity at shishaldin volcano, alaska. Journal of volcanology and geothermal research 151 (4), 365–381.

Power, J., Stihler, S., Chouet, B., Haney, M., Ketner, D., 2012. Seismic observations of redoubt volcano, alaska–1989-2010 and a conceptual model of the redoubt magmatic system. Journal of Volcanology and Geothermal Research 259, 31–44.

Power, J. A., Lahr, J. C., Page, R. A., Chouet, B. A., Stephens, C. D., Harlow, D. H., Murray, T. L., Davies, J. N., 1994. Seismic evolution of the 1989–1990 eruption sequence of redoubt volcano, alaska. Journal of volcanology and geothermal research 62 (1), 69–94.

Ripepe, M., Gordeev, E., 1999. Gas bubble dynamics model for shallow volcanic tremor at stromboli. Journal of Geophysical Research: Solid Earth (1978–2012) 104 (B5), 10639–10654.

Ruppert, N. A., Prejean, S., Hansen, R. A., 2011. Seismic swarm associated with the 2008 eruption of kasatochi volcano, alaska: Earthquake locations and source parameters. Journal of Geophysical Research: Solid Earth (1978–2012) 116 (B2).

Soosalu, H., Einarsson, P., Porbjarnardottir, B. S., 2005. Seismic activity related to the 2000 eruption of the hekla volcano, iceland. Bulletin of volcanology 68 (1), 21–36.

Sparks, R. S. J., 2003. Forecasting volcanic eruptions. Earth and Planetary Science Letters 210 (1), 1–15.

Sparks, R. S. J., Biggs, J., Neuberg, J. W., 2012. Monitoring volcanoes. Science 335 (6074), 1310–1311.

Stelling, P., Beget, J., Nye, C., Gardner, J., Devine, J., George, R., 2002. Geology and petrology of ejecta from the 1999 eruption of shishaldin volcano, alaska. Bulletin of volcanology 64 (8), 548–561.

Vergniolle, S., Boichu, M., Caplan-Auerbach, J., 2004. Acoustic measurements of the 1999 basaltic eruption of shishaldin volcano, alaska: 1. origin of strombolian activity. Journal of volcanology and geothermal research 137 (1), 109–134.

Vergniolle, S., Caplan-Auerbach, J., 2004. Acoustic measurements of the 1999 basaltic eruption of shishaldin volcano, alaska: 2. precursor to the subplinian phase. Journal of volcanology and geothermal research 137 (1), 135–151.

Voight, B., 1988. A method for prediction of volcanic eruptions. Nature 332, 125–130.

Voight, B., Hoblitt, R., Clarke, A., Lockhart, A., Miller, A., Lynch, L., McMahon, J., 1998. Remarkable cyclic ground deformation monitored in real-time on montserrat, and its use in eruption forecasting. Geophysical Research Letters 25 (18), 3405–3408.

Zecevic, M., De Barros, L., Bean, C. J., OBrien, G. S., Brenguier, F., 2013. Investigating the source characteristics of long-period (lp) seismic events recorded on piton de la fournaise volcano, la réunion. Journal of Volcanology and Geothermal Research 258, 1–11.

Highlights

- We analyzed the evolution of Shishaldin volcano Long Period seismicity in 2003-04.
- We found a source deepening and then a shallowing until a small eruption.
- We link source depth variations with pressure changes within the plumbing system.
- We imputed these changes to a magma intrusion from a deeper to a shallower chamber.
- This study shows the LP potential to infer physical chances in magmatic systems.